Hypersonic Waveriders for Planetary Atmospheres

John D. Anderson Jr.,* Mark J. Lewis,† and Ajay P. Kothari‡
University of Maryland, College Park, Maryland 20742
and
Stephen Corda§
Johns Hopkins Applied Physics Laboratory, Laurel, Maryland 20702

The concept of a hypersonic waverider for applications in foreign planetary atmospheres is explored, particularly in regard to aeroassist for space vehicle trajectory modification. The overall concept of hypersonic waveriders is discussed in tutorial fashion. A partial review of past work is given, and the role of a new family of waveriders—the viscous optimized waveriders generated at the University of Maryland—is highlighted. The mechanics of trajectory modification by aerodynamic vehicles with high lift-to-drag ratios in planetary atmospheres is explored. Actual hypersonic waverider designs for Mars and Venus atmospheres are presented. Moreover, they exhibit very high lift-to-drag ratios, as high as 15 in the atmosphere of Venus. These results graphically demonstrate that a hypersonic waverider is a viable candidate for aeroassist maneuvers in foreign planetary atmospheres.

Nomenclature

C = CFL constant
C_D = drag coefficient
C_L = lift coefficient
C_f = skin friction coefficient
D = drag
E = first Euler vector
G = second Euler vector
H = third Euler vector
h = altitude
L = lift
M = Mach number
m = secondary body mass
$\dot{m}$ = mass flow
Re = Reynolds number
r = orbital radius, radial dimension
T = temperature
t = time variable
V = velocity magnitude
$\bar{V}$ = normalized velocity
x = linear dimension
z = axial coordinate
β = shock angle
γ = ratio of specific heats
ΔV = change in velocity magnitude
δ = orbital angular deflection
μ = coefficient of viscosity
Θ = angle of arc through atmosphere
θ = surface angle of obliquity
ρ = density
ν = gravitational constant times mass
ψ = stream function
ω = viscosity temperature exponent

Subscripts
c = circular orbit value
o = reference value
p = value at periapsis
t = stagnation conditions
w = wall value
1 = initial or approach
2 = final or exit
∞ = value at infinite distance

Introduction

THE use of aerodynamic forces to tailor trajectories and orbits of space vehicles has been considered since 1961 when London[1] suggested the use of aerodynamic forces to execute an orbital plane change. Extensions of this work have been surveyed by Walberg,[2-4] who listed three possibilities for the useful application of aerodynamic forces during the flight of space vehicles. The first of these, synergetic plane change, is described above in conjunction with Ref. 1. This makes use of aerodynamic lift and minimum aerodynamic drag, hence emphasizing the importance of a high lift-to-drag ratio, L/D, for the space vehicle. Aerocapture is another application, in which aerodynamic drag is used to dissipate the excess hyperbolic velocity of a space vehicle entering a planetary atmosphere from deep space, allowing the vehicle to be captured by the gravitational field of the planet, placing it in the desired orbit about the planet. The final category is orbital transfer, in which a vehicle in high Earth orbit returns to the Earth's atmosphere and uses aerodynamic drag to achieve a low Earth orbit. For the most part, these applications make use of aerodynamic drag, although some lift is considered in the first application.

An application where aerodynamic lift is the primary concern has been recently described by Randolph and McRonald,[5] who suggest the trajectory modification of a close-approach solar probe by passing through the terrestrial or Cytherean (i.e., Venusian) atmospheres. Here, a conventional gravity assist trajectory can be greatly magnified by an aerodynamic assist, using the vehicle's lift vector to obtain virtually any amount of angular deflection change of the trajectory as the vehicle passes through the planetary atmosphere. Of course, drag during this atmospheric pass must be minimized so that losses of velocity magnitude do not offset the gains accomplished by the angular deflection. Hence, for such an application, it is extremely important that the space vehicle has as

Presented as Paper 90-0538 at the AIAA 28th Aerospace Sciences Meeting, Reno, NV, Jan. 8-11, 1990; received Jan. 12, 1990; revision received Sept. 18, 1990; accepted for publication Sept. 26, 1990.

*Professor, Department of Aerospace Engineering. Fellow AIAA.
†Assistant Professor, Department of Aerospace Engineering. Member AIAA.
‡Research Engineer, Department of Aerospace Engineering. Member AIAA.
§Research Engineer. Member AIAA.

large a lift-to-drag ratio as possible. Randolph and McRonald call for L/D ratios on the order of 10, and suggest that a hypersonic waverider might be able to provide such values. However, no analysis of such a waverider is presented in Ref. 5.

The importance of high L/D for hypersonic aerodynamic assist of space vehicles is particularly underscored by Lewis and Kothari.[6] Here, closed-formed equations for an aeroassisted and modified hyperbolic trajectory are derived and presented as a function of L/D. These equations clearly show the importance of high L/D for such trajectory modification, demonstrating among other variations that the maximum angular deflection of the trajectory through an atmosphere is directly proportional to L/D, and that the atmospheric exit velocity at the end of the vehicle's transit through the atmosphere is an exponential formulation, with increasing L/D ratio serving to decrease the velocity decrement during transit through the atmosphere.

Lewis and Kothari demonstrated that a waverider shape has a reasonable potential for achieving high enough values of L/D to be useful for such an aeroassist role; indeed, a waverider may be the only hypersonic configuration that produces the required high L/D ratios.

The purpose of the present paper is to examine in more detail the aerodynamic performance of waveriders in planetary atmospheres, and to present for the first time actual optimized waverider shapes designed specifically for transit through the atmospheres of Mars and Venus. This paper is intended to provide a general tutorial review on the general concept of hypersonic waveriders, including an overview of some of the literature. It will also explain the importance of high L/D for space vehicle aeroassist trajectories, and the generation of actual waverider configurations for transits through the Martian and Cytherean atmospheres will be presented and discussed.

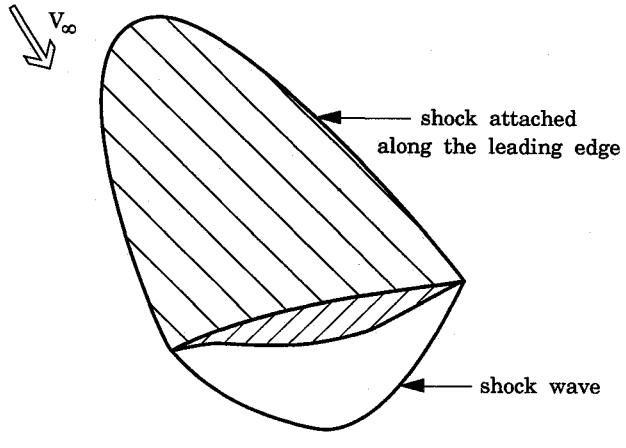

a) Waverider

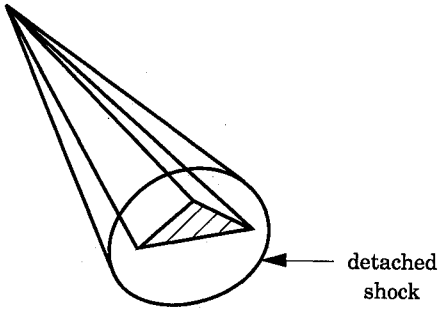

b) Generic Vehicle

Fig. 1 Comparison of waverider and generic hypersonic configuration.

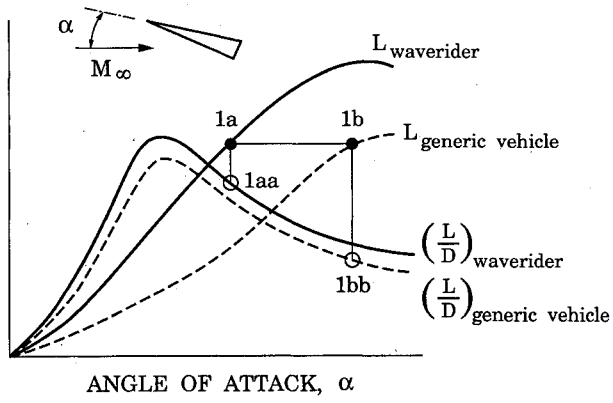

Fig. 2 Comparison between lift and L/D curves for a waverider and a generic vehicle.

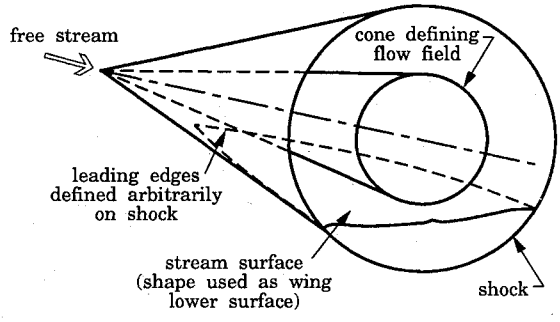

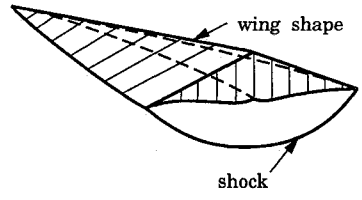

Fig. 3 Cone flow wing (from Ref. 21).

General Concept of the Waverider—A Review

Waveriders: What Are They?

A waverider is a supersonic or hypersonic vehicle that has an attached shock wave all along its leading edge at design point conditions, as sketched in Fig. 1a. Because of this, the vehicle appears to be riding on top of its shock wave—hence the term "waverider." This is in contrast to a more conventional hypersonic vehicle, where the shock wave is usually detached from the leading edge, as sketched in Fig. 1b. The aerodynamic advantage of the waverider in Fig. 1a is that the high pressure behind the shock wave under the vehicle does not "leak" around the leading edge to the top surface; the flowfield over the bottom surface is contained, and the high pressure is preserved. In contrast, for the vehicle shown in Fig. 1b, there is communication between the flows over the bottom and top surfaces; the pressure tends to "leak" around the leading edge, and the general integrated pressure level on the bottom surface is reduced, resulting in less lift. Because of this, the generic vehicle in Fig. 1b must fly at a larger angle of attack α to produce the same lift as the waverider in Fig. 1a. This is illustrated in Fig. 2, where the lift curves (L vs α) are sketched for the two vehicles in Fig. 1. At the same lift, points 1a and 1b in Fig. 2 represent the waverider and generic vehicles, respectively. Also shown in Fig. 2 are typical variations of L/D vs α, which for slender hypersonic vehicles are not too

different for the shapes in Fig. 1a and 1b. However, note that because the waverider generates the same lift at a smaller α (point 1a in Fig. 2,) the L/D for the waverider is considerably higher (point 1aa) than that for the generic shape (point 1bb).

Another characteristic of waveriders is that they are generated from known flowfields established by other basic shapes different from that of the waverider itself. For example, Fig. 3 illustrates a waverider generated from a conical flowfield. A cone, along with the conical shock wave attached at the vertex of that cone, is sketched at the top of Fig. 3. Any stream surface of this conical flowfield downstream of the shock can be used as the surface of the waverider; in so doing, the shock wave will be attached all along the leading edge of the waverider, as shown at the bottom of Fig. 3. Moreover, the attached shock wave on the resulting waverider will, of course, be a segment of the conical shock wave shown at the top of Fig. 3.

A Brief Review of the Literature

The waverider concept was first introduced by Nonweiler in 1959.[7] Over the years since its inception,[7-12] the concept of the waverider has received sporadic attention, with the majority of the research carried out in Europe. An excellent and authoritative survey of waverider research has been given by Townend[8]; this paper is recommended as a starting point for anyone not familiar with the field. A tutorial approach is also taken by Roe.[10] As mentioned earlier, waveriders are generated from known flowfields; those generated from the flow behind a wedge are discussed by Nonweiler.[7] The first extension to the use of a conical flow as a generating flowfield is discussed in Ref. 11. Rasmussen and his colleagues at the University of Oklahoma (see, for example, Refs. 12-14) utilized hypersonic small disturbance theory to design waveriders from flowfields over right-circular cones as well as elliptic cones. During the early 1980s, Rasmussen's work constituted the main focus of waverider research in the United States. In this work, the calculus of variations was used to optimize the waverider shape utilizing the inviscid properties of the flow only. Other work of a similar nature was carried out by Cole and Zien[15] and Schindel.[16] Baron[17] investigated the interesting aspect of using two or more adjacent cones to generate a more complex flowfield from which waveriders could be obtained.

In all of the above work, the waverider configurations were designed (and sometimes optimized) on the basis of inviscid flowfields. In turn, the drag predicted by such inviscid analyses was simply wave drag, and the resulting inviscid L/D looked promising. However, waveriders tend to have large wetted surface areas, and the skin-friction drag, always added to the waverider aerodynamics after the fact, tended to greatly

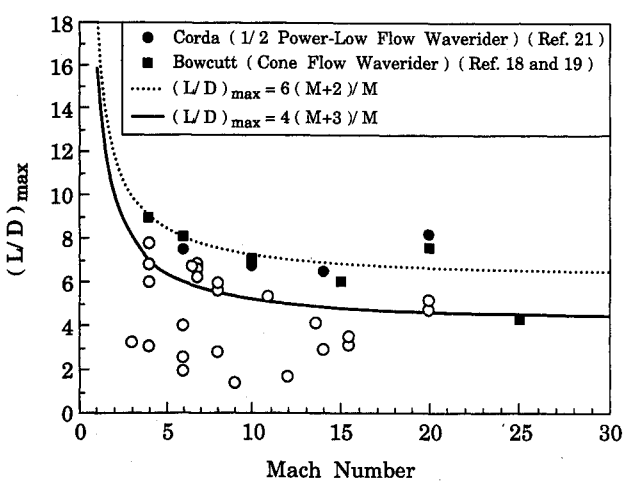

Fig. 4 Maximum lift-to-drag ratio comparison for various hypersonic configurations.

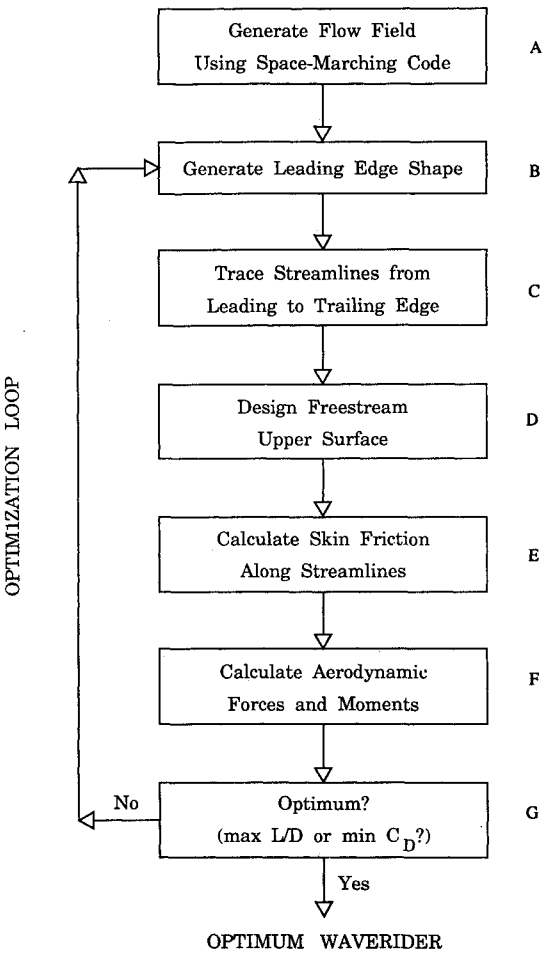

Fig. 5 Waverider design process.

decrease the predicted inviscid L/D ratio. This made the waverider a less interesting prospect, and led to a lack of interest—indeed outright skepticism—by researchers, particularly in the United States. On the other hand, recent work at the University of Maryland has taken a different tact. A new family of waveriders has been generated wherein the skin-friction drag is included within an optimization routine to calculate waveriders with maximum L/D. In this fashion, the tradeoffs between wave drag and friction drag are accounted for during the optimization process, and the resulting family of waveriders has shape and wetted surface area so as to optimize L/D. This family of waveriders is called viscous-optimized hypersonic waveriders. The first work on these waveriders was carried out by Bowcutt et al.[18-20] Here, the generating inviscid flowfield was conical, and the viscous shear stress was calculated by means of an integral boundary-layer technique. A second generation of viscous optimized waveriders was studied by Corda and Anderson[21] wherein a power-law minimum drag body was used for the generating flowfield, and a reference temperature method was employed for the calculation of skin friction. The viscous optimized waveriders presented in Refs. 18-21 have very high hypersonic L/D ratios. This is illustrated in Fig. 4, where maximum L/D is plotted vs Mach number for a variety of hypersonic vehicles; the open symbols pertain to different shapes wherein the L/D is obtained by either calculation, wind tunnel experiments, or flight test, all pertaining to different Reynolds numbers. (For an itemization of the references associated with each of the open symbols in Fig. 4, see Ref. 22.) Note that, in general, L/D decreases with increasing Mach number; the solid curve in Fig. 4 is an empirically based upper limit for L/D set by Kuchemann,[23] and can be interpreted loosely as a type of "L/D barrier." The solid symbols correspond to the viscous optimized waveriders reported by Bowcutt, Corda, Anderson,

and Capriotti in Refs. 18–22; these waveriders obviously "break" the L/D barrier. Finally, these viscous optimized waveriders have been recently tested in the unitary wind tunnel at the NASA Langley Research Center, and the preliminary experimental data confirms the University of Maryland design point calculations.[24] Hence, the work in Refs. 18–22 is beginning to be experimentally verified and validated.

Waverider Analysis

The analysis and optimization of waveriders from general axisymmetric flowfields require distinct capabilities. First, one must be able to generate a "known" axisymmetric flowfield. Then one must analyze the waverider generated from the flowfield, which involves: 1) the evaluations of the aerodynamic coefficients (e.g., C_L, C_D, and C_M) and 2) the determination of the parameters that describes the waverider geometry. Finally, waverider optimization requires finding the set of parameters that yield the desired figure of merit (e.g., maximum L/D or minimum C_D). The breakdown of the waverider design process is shown in Fig. 5. The contents of each box will be discussed in the following paragraphs. A more detailed description of the design process is given in Ref. 22.

Generation of Inviscid Flowfield

The calculation of the "known" axisymmetric flowfield will be discussed first. Separate techniques are used for the case of 1) flow over a right circular cone and 2) flow over a general axisymmetric body, as described below.

Conical Flow

For the case of conical flow, the Taylor-Maccoll equation shown below is solved using a standard fourth-order Runge-Kutta method, as given in Ref. 25:

$$\frac{\gamma-1}{2}\left[1-V_r^2-\left(\frac{dV_r}{d\theta}\right)^2\right]\left[2V_r+\frac{dV_r}{d\theta}\cot\theta+\frac{d^2V_r}{d\theta^2}\right]-\frac{dV_r}{d\theta}\left[V_r\frac{dV_r}{d\theta}+\frac{dV_r}{d\theta}\frac{d^2V_r}{d\theta^2}\right]=0 \tag{1}$$

In Eq (1), V_r is the nondimensional component of flow velocity along a conical ray, θ is the angle of the ray referenced to the cone axis, and γ is the ratio of specific heats.

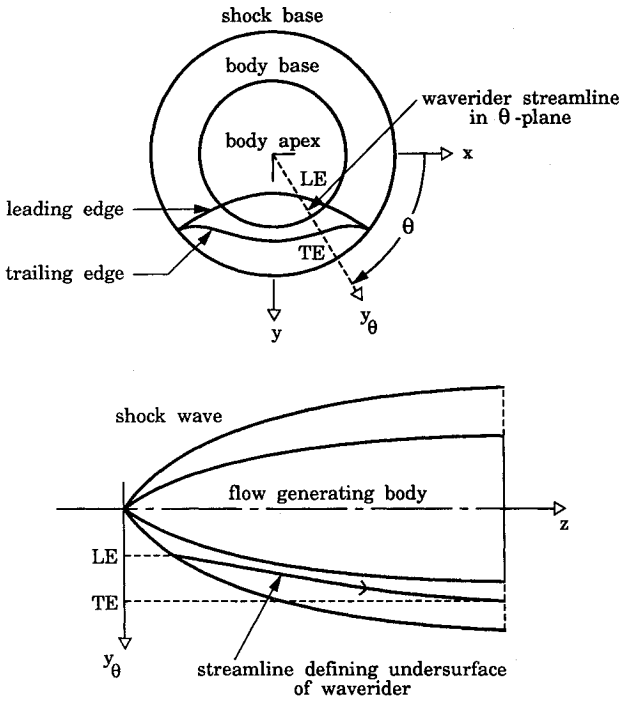

Fig. 6 Waverider construction.

General Axisymmetric Flowfield

For an inviscid axisymmetric flowfield in general, the governing partial differential equations are the Euler equations given below:

$$\frac{\partial G}{\partial z}=-\frac{\partial E}{\partial r}-H \tag{2}$$

where

$$G=\begin{bmatrix}\rho w\\ p+\rho w^2\\ \rho vw\end{bmatrix}\quad E=\begin{bmatrix}\rho v\\ \rho vw\\ p+\rho v^2\end{bmatrix}\quad H=\frac{1}{r}\begin{bmatrix}\rho v\\ \rho vw\\ \rho v^2\end{bmatrix} \tag{3}$$

in which ρ is the density, w is the axial (z) component of the flow velocity, v is the transverse (r) component of the flow velocity, and p is the pressure. These equations are solved numerically using MacCormack's explicit space-marching finite-difference scheme. (See Refs. 26 and 27 for a basic discussion of MacCormack's technique.)

Generation of Leading-Edge Shapes

Once the flowfield is calculated, waverider shapes can be "carved" out of the flowfield, as shown in Fig. 6. As is seen in this figure, the leading-edge curve is traced back along the streamlines of the flowfield to generate the lower surface of the waverider. Note that the projection of the leading-edge curve in the cross-stream (x-y) plane uniquely defines a waverider geometry for a given flowfield. The leading-edge curves are generated by the optimization process, as will be discussed shortly.

Streamline Tracing

Streamlines are traced from the leading edge, through the "known" flowfield, to create the waverider lower surface. The manner of this streamline tracing is based on a stream function method, as discussed by Corda,[22] which should be consulted for further elaboration.

Freestream Upper Surface

The upper surface is created by simply following the freestream back through the given leading-edge curve to the base of the waverider. The pressure on this freestream upper surface is the freestream pressure, p_∞.

Skin Friction Calculations

The skin friction distribution along the streamlines that form the waverider is calculated using the reference temperature method of Eckert.[28] In the reference temperature method, approximate formulas are used to predict the skin friction, with the physical properties evaluated at an appropriate reference temperature. For a flat plate in laminar flow, the local skin friction coefficient is given by

$$C_f=0.664\frac{1}{\sqrt{Re_x}}\frac{T'^{(\omega-1)/2}}{T_\infty} \tag{4}$$

with Re_x as the local Reynolds number, defined as

$$Re_x=\frac{\rho_\infty V_\infty x}{\mu_\infty} \tag{5}$$

where ρ_∞ is the freestream density, V_∞ is the freestream velocity, x is the local distance from the leading edge of the plate, and μ_∞ is the freestream value of the viscosity.

Also in Eq. (4), T' is the reference temperature, defined as

$$\left(\frac{T'}{T_\infty}\right)=1+0.032M_\infty^2+0.58\left(\frac{T_w}{T_\infty}-1\right) \tag{6}$$

where M_∞ is the freestream Mach number and T_w is the wall temperature. Finally, ω in Eq. (4) is the exponent of an assumed exponential variation of μ, namely,

$$\left(\frac{\mu'}{\mu_\infty}\right) = \left(\frac{T'}{T_\infty}\right)^\omega \tag{7}$$

A value of $\omega = 0.75$ is used in the present study.

The flat plate skin friction coefficient for turbulent flow is given by

$$C_f = \frac{0.0592}{(Re_x')^{0.2}} \tag{8}$$

where

$$Re_x' = \frac{\rho' V_\infty x}{\mu'} \tag{9}$$

In Eq. (9), ρ' and μ' are evaluated at the reference temperature T'.

This type of skin friction analysis is much simpler, in concept and use, than integral boundary-layer methods. Results obtained using the reference temperature method were within 10% of results determined using a more complex integral boundary-layer method, Ref. 18, even at high hypersonic Mach numbers. Also, the computation time required by the reference temperature method is very small when compared with an integral boundary-layer method.

Boundary-layer transition is predicted using a correlation of the local transition Reynolds number $Re_{x,t}$ with the local edge Mach number M_e, as follows

$$\log_{10} Re_{x_t} = 6.421 \exp[1.209x10^{-4} M_e^{2.641}] \tag{10}$$

This correlation is based on the experimental data of Di-Cristina[29] for transition on sharp cones at 0-deg angle of attack. This correlation is used due to the lack of better methods of transition prediction in hypersonic flows.

Aerodynamic Forces and Moments

The aerodynamic force and moment coefficients are calculated by numerically integrating the pressure and shear stress over the surface of the waverider. Base drag is not calculated. Details of the integration for the forces and moments can be found in Ref. 22.

Waverider Optimization

The construction and aerodynamic analysis of a single waverider configuration is shown by blocks A-F in Fig. 5, and just described in the previous paragraphs. Now, the optimization is performed by perturbing the shape of the leading-edge curve (which corresponds to a unique waverider geometry), until a configuration is found with the optimum value of the specified figure of merit—either maximum L/D or minimum total drag, as in the present analysis. The nonlinear simplex method of Nelder and Mead[30] is used for the numerical optimization. For more details of the simplex method as applied to the waverider analysis, see Refs. 18–22.

Waverider Applications in Planetary Atmospheres—Mechanics of Trajectories and Orbits

Orbit Modification and L/D Requirements

To determine the L/D requirements for an aeroassisted maneuvering vehicle, it is worth considering the effect that L/D has on the performance of a particular mission profile. Obviously, the L/D required for a given vehicle will be highly dependent on the mission, and it is, therefore, difficult to draw generalities without a specific trajectory in mind. As a demonstration of the importance of L/D, an example of the use of a waverider for orbital maneuvering is considered for the case of hyperbolic gravity assist trajectory past a gravitating body, as is commonly used for ΔV increments on planetary missions.

Without an aeroassist, the maneuver is represented by a simple hyperbolic orbital trajectory.[31] A probe at incoming relative velocity V_∞ approaches a primary gravitational source, such as a planet, and accelerates to velocity

$$V(r) = \sqrt{V_\infty^2 + \frac{2\nu}{r}} \tag{11}$$

where $\nu = GM_{\text{primary}}$, the gravitational constant times the mass of the primary body.

The probe leaves the planet and returns to velocity V_∞ at distance $r = \infty$, having turned through an angle of

$$\delta = 2 \sin^{-1}\left[\frac{1}{1 + (r_p V_\infty^2/\nu)}\right] \tag{12}$$

where r_p is the radius at periapsis, or closest approach.

A trajectory with an atmospheric passage provides unlimited capability to modify the flight direction, with the constraint that velocity magnitude is lost to drag during the course of the flight. A vehicle entering the atmosphere will experience a deceleration of

$$dV = -\frac{D}{m}\,dt \tag{13}$$

where D/m is the drag force divided by the vehicle mass. Since it is most convenient to characterize the vehicle in terms of the lift-to-drag ratio L/D this is written as

$$dV = -\frac{L}{(L/D)m}\,dt \tag{14}$$

The time of flight can be related to the arc length Θ traveled at radius r in the atmosphere since $V dt = r d\Theta$. If it is assumed that approximately constant-altitude flight is to be achieved, lift must be used to add to gravitational forces in counteracting the excess centrifugal effects. This means that the waverider is flying "upside-down" with respect to the planet's surface, using its lift to stay in the atmosphere:

$$L + \frac{\nu m}{r^2} = \frac{mV^2}{r} \tag{15}$$

so that Eq. (14) can be written as

$$dV = -\left[\frac{L}{D}\right]^{-1}\left(V - \frac{\nu}{rV}\right)d\Theta \tag{16}$$

Note that positive lift augments gravity, so it is acting toward the planet.

The vehicle will therefore travel through an angle Θ at altitude r, where

$$\Theta = -\left[\frac{L}{D}\right]\int_{V_1}^{V_2} \frac{dV}{V - (\nu/rV)}$$

$$= -\frac{1}{2}\left[\frac{L}{D}\right] \ln\left\{\frac{V_2^2 - (\nu/r)}{V_1^2 - (\nu/r)}\right\} \tag{17}$$

in which it is assumed that L/D is approximately constant or, at least, can be characterized by some constant value during the flight. Equation (17) can be rewritten to express the velocity change as a function of sweep angle:

$$V_2 = \sqrt{\exp\left[\frac{-2\Theta}{(L/D)}\right]V_1^2 - \left\{\exp\left[\frac{-2\Theta}{(L/D)}\right] - 1\right\}\frac{\nu}{r}} \tag{18}$$

Table 1 Atmospheric entry parameters

Planet	Sonic speed, m/s	V_{rotation}, km/s	V_{esc}, km/s	$M_{\text{esc}}/M_{\text{corr}}$	V_{circ}, km/s	$M_{\text{circ}}/M_{\text{corr}}$	$T_{l,\text{esc}}$	T_l
Earth	300	0.46	11.18	37/36	7.91	26/25	2.0	1
Venus	248	0.002	10.37	42/42	7.33	30/30	1.5	0
Mars	192	0.24	5.03	26/25	3.56	19/17	0.4	0
Jupiter	914	12.80	59.37	65/51	41.98	46/32	3.0	1
Saturn	735	10.27	35.54	48/34	25.13	34/20	1.2	0
Uranus	578	2.58	21.31	36/32	15.07	26/22	0.4	0
Neptune	563	2.68	23.78	42/37	16.81	30/25	0.5	0

Since we are ultimately interested in the velocity at escape from the planet, we can use Eq. (11) to express the final velocity at infinity in terms of the initial relative approach velocity:

$$V_{\infty 2}=\sqrt{\exp\left[\frac{-2\Theta}{(L/D)}\right]V_{\infty 1}^2+\left\{\exp\left[\frac{-2\Theta}{(L/D)}\right]-1\right\}\frac{\nu}{r}} \tag{19}$$

Note that drag in the planetary atmosphere has decreased the incoming velocity by an amount governed by the exponential scale factor $2\Theta/(L/D)$. Increasing lift-to-drag ratio results in a proportional increase in the angle that can be traversed in the atmosphere for a given loss in velocity. Reference 6 explores the ramifications of these results in greater detail.

For interplanetary probes that would use atmospheres of these planets for trajectory changes or for preplanned kinetic energy losses, the assumption of constant L/D is quite valid. For such cases, the incoming velocities are generally much greater than the planet's circular velocities and, hence, high negative values of lift (or L/D) are always required to maintain force balance.

A glance at Eq. (17) shows that for $V_2=\sqrt{\nu/r}$, Θ goes through a singularity. This is because at velocities equivalent to the circular velocities, no lift is required to maintain the force balance between the gravitational and the centrifugal forces. Hence, the assumption of constant L/D forces drag to go through zero, which is not correct. In fact, the solution should drive L/D to zero, contrary to the constant value assumption.

For cases where L/D must be a variable, the above formulation can be modified. This is applicable, for example, to atmospheric trajectories with Hohmann transfers from parking orbits, which are close to the planet but are outside the atmosphere. In these cases, a small amount of lift is required to maintain the force balance (negative at first and positive later on). For such case, L/D will go through zero during the transition, going from negative to positive values of lift. Here, the angle of attack will always be small, since the lift vector is of small magnitude. It can, therefore, be assumed that the drag coefficient C_D variation occurs inside the so-called drag bucket, and so is almost a constant.

Substituting for drag as $D=\frac{1}{2}\rho V^2 S C_D$ in Eq. (13),

$$\frac{dV}{V}=-\frac{1}{2}\frac{C_D\rho S}{m}r\,d\Theta \tag{20}$$

which integrates to

$$V(\Theta)=V_1\exp\left[-\frac{1}{2}\frac{C_D\rho S r\Theta}{m}\right] \tag{21}$$

Writing the lift as $L=D(L/D)$ in Eq. (15) and substituting for drag in terms of C_D,

$$\frac{L}{D}=\frac{2m}{C_D r\rho S}\left(\frac{\nu}{r}\frac{1}{V^2}-1\right) \tag{22}$$

substituting for V, and recognizing once again that the circular orbit velocity $V_c=\sqrt{\nu/r}$,

$$\frac{L}{D}=\frac{2m}{C_D r\rho S}\left\{\left(\frac{V_c}{V_1}\right)^2\exp\left[\frac{C_D\rho S r\Theta}{m}\right]-1\right\} \tag{23}$$

Here we have flipped the sign of lift, so that positive lift corresponds to upward force, and negative lift corresponds to downward force.

This formulation shows the variation of L/D that should be followed with the change in angle Θ as the vehicle goes around the planet. To start with, at $\Theta=0$, L/D will be negative, since V_c will always be less than the entry velocity V_1. For some value of Θ, L/D will be zero and then positive afterwards. Thus, the waverider will start out flying upside down at some angle of attack, will go through zero lift angle at some value of Θ, will roll 180 deg at this point to the right side up, and then fly with positive lift as its velocity drops below that of the circular velocity at that given radius. Equation (23), therefore, describes the variation of the angle of attack of the waverider with respect to the flight angle Θ as the waverider goes around the planet. It is also easy to see from this equation that a higher value of L/D translates directly into a greater distance that the vehicle can transverse around the planet (i.e., greater value of Θ).

Flight Environment

Table 1 presents the Mach numbers associated with atmospheric entry at planetary capture velocity and low planetary orbital velocity for several different planets. The first column indicates the speed of sound in the planetary atmosphere, calculated at the cloudtops of the Jovian planets and at a representative reentry altitude for Earth and Mars.

Note that both the Earth and Mars atmospheres are essentially isothermal in the altitudes of interest, so exact precision in specifying a flight trajectory for this comparison is not necessary. The Venus stratosphere temperature drops linearly from about 300 K at 50-km altitude to about 190 K at 80 km, after which it is nearly isothermal. For this plot, an entry altitude of 75 km was chosen based on proposed orbital missions of Ref. 5, but it should be remembered that the entry Mach number at Venus is a strong function of altitude. The second column of Table 1 indicates the planetary rotation speed, which, under certain conditions, might be subtracted from the entry speed to reduce the flight Mach number. A day on Venus lasts 5832 h, and so its rotational velocity is negligible compared to orbital speeds. Planet rotation is also insignificant for Earth and Mars, but it is significant for the outer planets.

Column 3 of Table 1 presents the velocity of capture into the planetary gravitational field, which is the escape velocity. The next column lists the corresponding Mach number for the capture velocity, along with the Mach number corrected for the planetary rotation. The last two columns list the same for atmospheric entry at the velocity characteristic of low planetary orbit, and the corresponding Mach numbers. Note that the correction for planetary rotation may not always be practi-

cal; for instance, such a benefit may not be realizable at Uranus, with its spin vector oriented towards the sun.

The last two columns of Table 1 present the stagnation temperatures of the freestream flow approaching a hypersonic vehicle at the Mach numbers characteristic of escape velocity and low orbital velocity without the rotational correction. These values have been normalized to the total temperature represented by flight at orbital velocity in Earth's atmosphere, which has been arbitrarily set to unity. This is an indication, albeit an imprecise one, of the heating levels to be encountered by a hypersonic vehicle. In reality, temperatures on a hypersonic vehicle will be governed by complicated chemical interactions; in the hypersonic regime, surface temperatures will not reach the flow stagnation temperature because of dissociation. However, the total temperature is an indication of the maximum energy available for heating the vehicle surface. Observe that the flow stagnation values are all within range of terrestrial experience, although actual heating comparisons would require more sophisticated analysis than is presented here. Note that transatmospheric vehicles operating in the terrestrial atmosphere will likely experience heating levels that are several times greater than those experienced during re-entry.[32]

Table 1 shows that the Mach number range for aeroassisted trajectories throughout the solar system matches that associated with hypersonic flight in Earth's atmosphere. As is indicated, low Earth orbital velocity is generally associated with flight at about Mach 26; higher Mach numbers would be encountered with entry from more energetic orbits or from capture. Indeed, Mach 26 is usually the quoted value for the upper range of transatmospheric flight for a vehicle such as the National Aerospace Plane. As a result, hypersonic vehicle design for Earth applications has focused on the range of Mach numbers between cruising flight at Mach 10 to single-stage-to-orbit acceleration flight of Mach 26.[33]

Although the actual velocities for atmospheric entry at the gas giants are high, the speed of sound of these planets' atmospheres and the fast rotation all help reduce the Mach number to a value similar to that for terrestrial transatmospheric flight.[34] Jupiter has the highest Mach number for low planetary orbit among the gas giants, but even this is not unreasonably high in comparison to Earth. In the Martian atmosphere, the low-orbit Mach number is actually somewhat below the upper range for flight on Earth. Mach numbers for entry into the Cytherean atmosphere are somewhat higher than comparable Earth-based values because of the generally

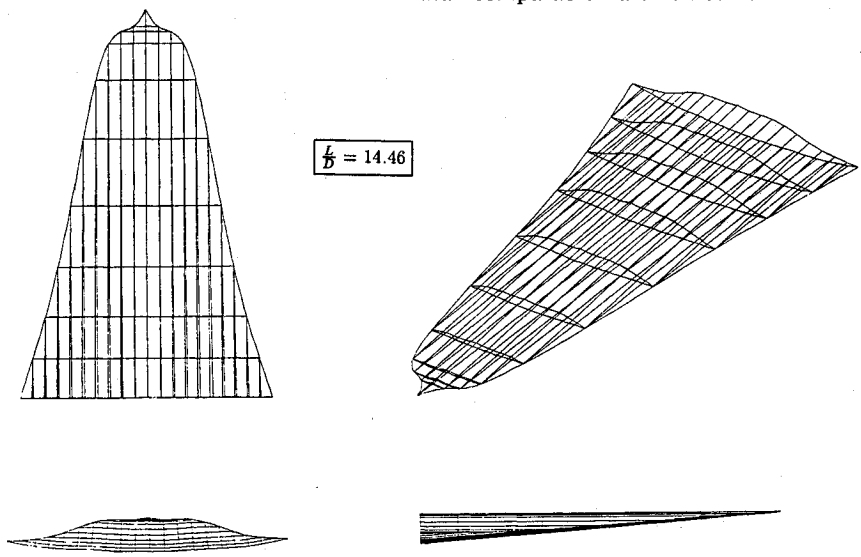

a) $h = 30$ km, $Re = 3.25 \times 10^{10}$

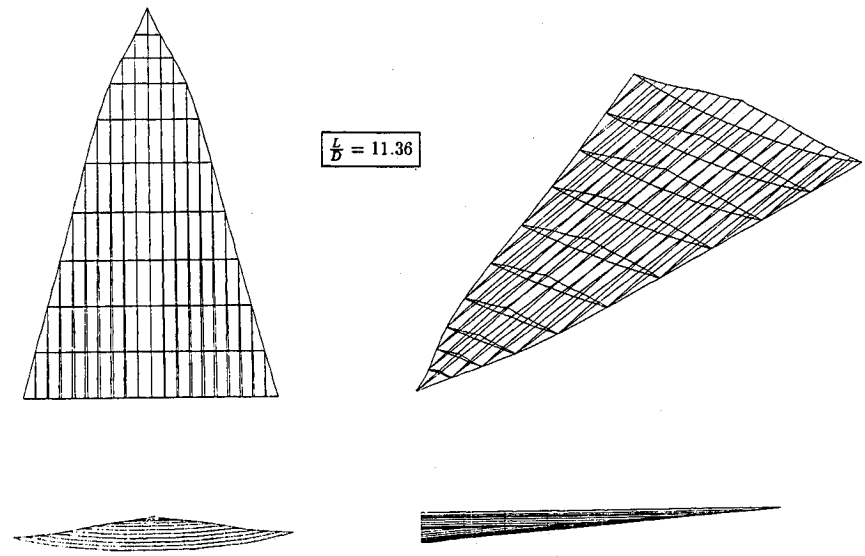

b) $h = 76$ km, $Re = 1.29 \times 10^{8}$

Fig. 7 Waverider designed for the atmosphere of Venus, $M_\infty = 30$, $\theta_{cone} = 5$ deg.

Table 2 Waverider lift and drag coefficients

Figure	Planet	M	θ, deg	Alt., km	Re	C_L	C_D	C_f	L/D
7a	Venus	30	5	30	3.25×10^{10}	0.0151	0.00104	1.72×10^{-5}	14.46
7b	Venus	30	5	76	1.29×10^{8}	0.0152	0.00133	0.000291	11.36
8a	Mars	19	7.5	20	1.03×10^{8}	0.0342	0.00515	0.0013	6.63
8b	Mars	19	7.5	30	2.51×10^{6}	0.0334	0.00629	0.00266	5.38

lower speed of sound. As will be discussed below, such effects will be minimized by the smaller value of γ associated with the CO_2 atmosphere of that planet. The Mach numbers characteristic of capture trajectories are also typically higher than those expected for transatmospheric flight on Earth, but are similar to values associated with aerobraking from geosynchronous orbit.

Viscous Optimized Waveriders for Planetary Atmospheres—Their Shapes and Aerodynamics

Using the analysis described for axisymmetric flowfields, a series of waverider configurations have been generated for flight within the Martian and Cytherean atmospheres. To the authors' knowledge, these represent the first waveriders to be designed for applications in foreign planetary atmospheres. The results described here are intended to examine only the general viability of waveriders for such an application—a detailed design and parametric study is left to future investigation. Here we simply ask the question: Can waveriders in foreign planetary atmospheres produce the magnitude of high L/D values required for mission applications? We will see that the answer appears to be a resounding yes.

In Figs. 7a and 7b, waveriders for the atmosphere of Venus are shown. Figure 7a is a point design for Mach 30 at an altitude of 30 km; Fig. 7b is a point design also at Mach 30, but at a higher altitude of 76 km. These waveriders were

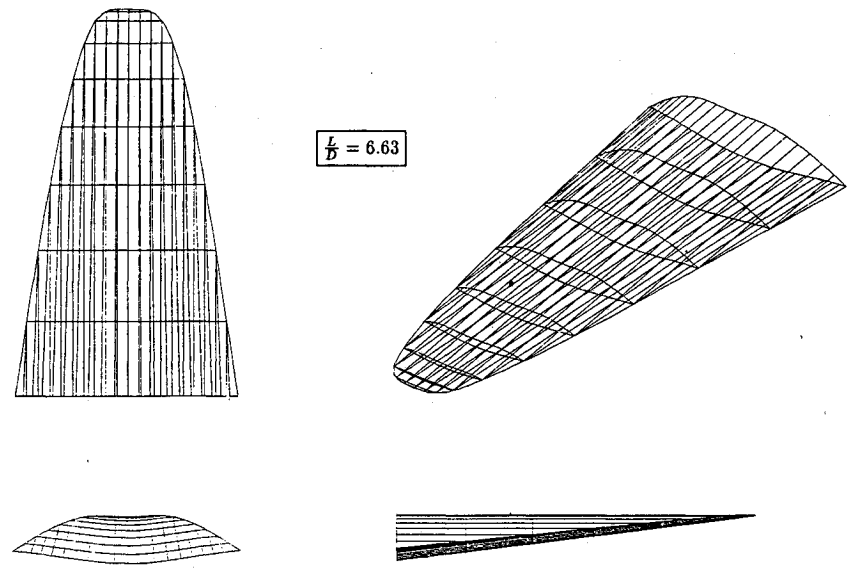

a) $h = 20$ km, $Re = 1.03 \times 10^7$

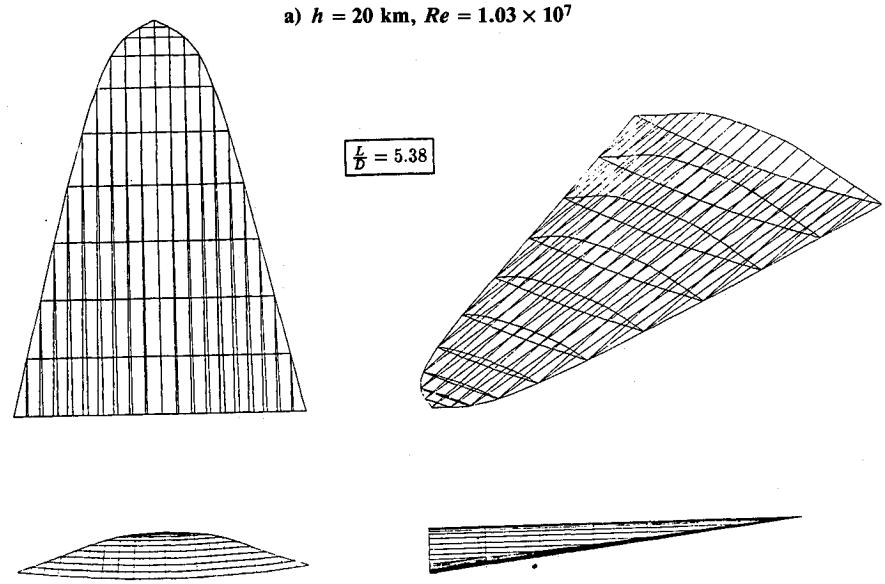

b) $h = 30$ km, $Re = 2.51 \times 10^6$

Fig. 8 Waverider designed for the atmosphere of Mars, $M = 19$, $\theta_{cone} = 7.5$ deg.

generated from the flowfield for a 5-deg half-angle cone. The wall temperature of the waverider was assumed to be $T_w = 1000$ K. The L/D ratio for the 30-km case (Fig. 7a) is 14.46—an exceptionally high value. Even at 76 km (Fig. 7b), the L/D is 11.36—also a high value. The primary reason for the high L/D values for the atmosphere of Venus is the high Reynolds numbers associated with the dense Cytherean atmosphere, and the resulting low skin-friction drag coefficients that accompany high Reynolds numbers. This will be elaborated upon shortly.

Waveriders for the Martian atmosphere are shown in Figs. 8a and 8b, for Mach 19 and altitudes of 20 and 30 km, respectively. Here, a 7.5 deg half-angle cone was used for the generating flowfield. The wall temperature was $T_w = 1000$ K. The L/D ratios were 6.63 and 5.38, respectively, for these two cases. These L/D values are considerably lower than those for Venus, again due to a Reynolds number effect associated with the low values of Re in the relatively thin Martian atmosphere.

More detailed information on the aerodynamic characteristics of these waveriders is given in Table 2. Here, M is Mach number, θ is the angle of the generating cone, the flowfield from which the compression surface of the waverider is obtained, C_L is the lift coefficient ($C_L = L/\frac{1}{2}\rho_\infty V_\infty^2 S$), C_D is the total drag coefficient ($C_D = D/\frac{1}{2}\rho_\infty V_\infty^2 S$) where D is composed of the sum of the wave drag (due to the pressure distribution over the surface) and the skin-friction drag (due to the shear stress distribution over the surface), C_f is the skin-friction drag coefficient itself, and, of course, L/D is the lift-to-drag ratio. Of particular note in this table are the low values of C_f for the Cytherean cases—simply due to the higher Reynolds numbers encountered in flight in the dense atmosphere of Venus. (Note that for all of the calculations in this paper, and hence for Table 2, the length of the waverider was chosen as 10 m.) It is also interesting to note that for most of the cases shown in Table 1, C_f is much smaller than C_D, indicating that the dominant drag mechanism for these viscous optimized waveriders is wave drag.

Emphasis is made that the waverider calculations in this paper assume a calorically perfect gas. Hence, the effect of the different chemical compositions of the atmospheres of Earth, Mars, and Venus is taken into account simply by the use of different values of the ratio of specific heat γ that pertain to those atmospheres. More sophisticated aspects, such as the details of chemically reacting flows, have not been included. This is justified by the recent work of McLaughlin,[35] which has shown that chemically reacting flowfield effects have minimal effect on the inviscid flows over hypersonic waveriders because of the generally small surface angles, and, hence, relatively weak shocks. In fact, chemically reacting effects may be important for the boundary-layer properties on a hypersonic waverider; this is an area for future investigation.

Finally, we note that the shapes of the waveriders shown in Figs. 7 and 8 for the atmospheres of Venus and Mars, respectively, do not, in general, differ greatly from those for the Earth's atmosphere, as presented in Refs. 18–22. The differences that are apparent are primarily due to the different values of Reynolds number and, to a lesser extent, the Mach number used in each case. Differences in the chemical composition of each atmosphere, as characterized by γ, has a minimal contribution to these variations.

Conclusions

In the present paper, we have

1) presented the first hypersonic waveriders designed for planetary atmosphere applications.

2) shown that high L/D values can be obtained, particularly for the case of flight through the atmosphere of Venus.

3) indicated that the use of Venus rather than Mars for an aeroassisted trajectory modification is preferable, due to the exceptionally high L/D values (as high as almost 15) obtained for Venus.

4) shown that the general, overall shapes of the waveriders designed for Earth, Mars, and Venus are essentially the same general configuration—no dramatic differences in shape occur.

Acknowledgments

The authors gratefully acknowledge the intellectual contributions of James Randolph and Angus McRonald of the Advanced Mission Group at the Jet Propulsion Laboratory, and Isaiah Blankson of the NASA Generic Hypersonics Program. Appreciation is also expressed to graduate students Charles Lind and Mary Kae Lockwood O'Neill, in the Department of Aerospace Engineering at the University of Maryland, for reviewing the text, and to Scott Seifert for his help in obtaining the graphical output of the waverider shapes.

References

[1]London, H. S., "Change of Satellite Orbit Plane by Aerodynamic Maneuvering," *Journal of the Aerospace Sciences,* Vol. 29, March 1962, pp. 323–332.

[2]Walberg, G. D., "The Next Generation of Reentry Vehicles—NASA's View," *Hypersonic Aerothermodynamics,* von Kármán Inst. Lecture Series Notes, Brussels, Belgium, Feb. 6–10, 1984, pp. 1–89.

[3]Walberg, G. D., "Aero-Assisted Orbit Transfer Window Opens on Missions," *Astronautics and Aeronautics,* Vol. 21, No. 11, Nov. 1983, pp. 36–43.

[4]Walberg, G. D., "A Survey of Aero-Assisted Orbital Transfer," *Journal of Spacecraft and Rockets,* Vol. 22, No. 1, Jan.–Feb. 1985, pp. 3–18.

[5]Randolph, J. E., and McRonald, A. D., "Solar Probe Mission Status," AAS/GSFC International Symposium on Orbital Mechanics and Mission Design, AAS Paper 89-212, Greenbelt, MD, April 24–27, 1989.

[6]Lewis, M. J., and Kothari, A. P., "The Use of Hypersonic Waveriders for Planetary Exploration," AIAA/JPL 2nd International Conference on Solar System Exploration, Pasadena, CA, Aug. 22–24, 1989.

[7]Nonweiler, T. R. F., "Aerodynamic Problems of Manned Space Vehicles," *Journal of the Royal Aeronautical Society,* Vol. 63, Sept. 1959, pp. 521–528.

[8]Townend, L. H., "Research and Design for Lifting Reentry," *Progress in Aerospace Sciences*, Vol. 19, No. 1, 1979, pp. 1–80.

[9]Coleman, G. T., "Aerodynamic Force Measurement on Caret and Delta Wings at High Incidence," *Journal of Spacecraft and Rockets*, Vol. 10, No. 11, Nov. 1973, pp. 750–751.

[10]Roe, P. L., "Theory of Waveriders," *Aerodynamic Problems of Hypersonic Vehicles,* edited by K. Enkenhus, J. F. Wendt, and R. C. Pankhurst, AGARD LS-42, 1972.

[11]Jones, J. G., Moore, K. C., Pike, J., and Roe, P. L., "A Method for Designing Lifting Configurations for High Supersonic Speeds, Using Axisymmetric Flow Fields," *Ingenieur—Archiv,* Vol. 37, June 1968, pp. 56–72.

[12]Rasmussen, M. L., "Waverider Configurations Derived from Inclined Circular and Elliptic Cones," *Journal of Spacecraft and Rockets,* Vol. 17, No. 6, Nov.–Dec. 1980, pp. 537–545.

[13]Kim, B. S., Rasmussen, M. L., and Jischke, M. C., "Optimization of Waverider Configurations Generated from Axisymmetric Conical Flows," AIAA Paper 82-1299, Jan. 1982.

[14]Broadway, R., and Rasmussen, M. L., "Aerodynamics of a Simple Cone Derived Waverider," AIAA Paper 84-0085, Jan. 1984.

[15]Cole, J. D., and Zien, T. F., "A Class of Three-Dimensional Optimimum Hypersonic Wings," *AIAA Journal,* Vol. 7, Feb. 1969, pp. 264–271.

[16]Schindel, L. H., "High Lift/Drag Ratio Hypersonic Missiles," Internal Memorandum, Weapons Dynamics Div., Naval Surface Weapons Center, Silver Spring, MD, 1980.

[17]Baron, J. R., "Configuration Definition Based on Intersecting Shock Surfaces," Dept. of Aeronautics and Astronautics, TR-81-1, Massachusetts Inst. of Technology, Cambridge, MA, May 1981.

[18]Bowcutt, K. G., Anderson, J. D., Jr., and Capriotti, D. P., "Viscous Optimized Hypersonic Waveriders," AIAA Paper 87-0272, Jan. 1987.

[19]Bowcutt, K. G., Anderson, J. D., Jr., and Capriotti, D. P., "Numerical Optimization of Conical Flow Waverider Including Detailed Viscous Effects," *Aerodynamics of Hypersonic Lifting Vehicles*, AGARD-CPP-428, March 1987, pp. 27/1–27/23.

[20]Bowcutt, K. G., "Optimization of Hypersonic Waveriders Derived from Cone Flows—Including Viscous Effects," Ph.D. Dissertation, Dept. of Aerospace Engineering, Univ. of Maryland, College Park, MD, 1986.

[21]Corda, S., and Anderson, J. D., Jr., "Viscous Optimized Hypersonic Waveriders Designed from Axisymmetric Flowfields," AIAA Paper 88-0369, Jan. 1988.

[22]Corda, S., "Viscous Optimized Hypersonic Waveriders Designed from Flows over Cones and Minimum Drag Bodies," Ph.D. Dissertation, Dept. of Aerospace Engineering, Univ. of Maryland, College Park, MD, 1988.

[23]Kuchemann, *The Aerodynamic Design of Aircraft,* Pergamon, Oxford, England, UK, 1978, pp. 448-510.

[24]Bauer, S., private communication, NASA Langley Research Center, Sept. 18, 1989.

[25]Zucrow, M. J., and Hoffman, J. D., *Gas Dynamics*, Wiley, New York, 1972.

[26]Anderson, J. D., Jr., *Modern Compressible Flow: With Historical Perspective*, McGraw-Hill, New York, 1st edition, 1982, 2nd edition, 1990.

[27]Anderson, J. D., Jr., *Hypersonic and High Temperature Gas Dynamics,* McGraw-Hill, New York, 1989.

[28]Eckert, E. R. G., "Engineering Relations for Heat Transfer and Friction in High-Velocity Laminar and Turbulent Boundary-Layer Flow Over Surfaces With Constant Pressure and Temperature," *Transactions of the ASME*, Vol. 78, No. 6, Aug. 1956.

[29]DiCristina, V., "Three-Dimensional Laminar Boundary Transition on a Sharp 8 Degree Cone at Mach 10," *AIAA Journal*, Vol. 8, May 1970, p. 855.

[30]Nelder, J. A., and Mead, R., "A Simplex Method for Function Minimization," *Computer Journal*, Vol. 7, Jan. 1965, pp. 308-313.

[31]Kaplan, M. H., *Modern Spacecraft Dynamics and Control,* Wiley, New York, 1976, pp. 92-96.

[32]Tauber, M. E., and Meneses, G. P., "Aerothermodynamics of Transatmospheric Vehicles," AIAA Paper 86-1257, Jan. 1986.

[33]Vinh, Busemann, and Culp, *Hypersonic and Planetary Entry Flight Mechanics,* Univ. of Michigan Press, Ann Arbor, MI, 1980.

[34]Kondratyev, K. Y., and Hunt, G. E., *Weather and Climate on Planets,* Pergamon, Oxford, England, UK, 1982, pp. 406-409.

[35]McLaughlin, T., "Viscous Optimized Hypersonic Waveriders for Chemical Equilibrium Flow," M.S. Thesis, Rept. UM-AERO-90-17, Dept. of Aerospace Engineering, Univ. of Maryland, College Park, MD, 1990.

Walter B. Sturek
Associate Editor